# LOCAL DEBRIS CONGESTION IN THE GEOSYNCHRONOUS ENVIRONMENT WITH POPULATION AUGMENTATION

**P. Anderson and H. Schaub**

*University of Colorado, Boulder, CO, 80309, USA, Email: paul.anderson@colorado.edu*

## ABSTRACT

Forecasting of localized debris congestion in the geostationary (GEO) ring is performed to investigate how frequently near-miss events occur for every longitude slot at GEO. A parallelized propagation routine is used to propagate the current resident space object (RSO) population at GEO forward in time, and representative augmentation of this population is implemented to simulate congestion in "business-as-usual" launch traffic, with and without mitigation at end-of-life. Congestion forecasting for a 50-year time frame is presented to illustrate the need for both appropriately-executed mitigation and active remediation measures at GEO.

Key words: Geosynchronous orbit; debris forecasting.

## 1. INTRODUCTION

The geostationary (GEO) ring is a unique commodity of the terrestrial satellite industry that is becoming increasingly contaminated with orbit debris [1, 2, 3]. As the lack of atmospheric drag effects at the GEO altitude renders the lifetimes of these debris infinitely long [4, 5, 6], conjunction and mitigation assessment must be performed to safeguard operational GEO satellites from colliding with the debris population. As GEO satellites must maintain a specific longitude, analysis of the *macroscopic* behavior of the GEO debris field is required to describe debris fluxes through particular GEO longitude slots, to forecast how frequently operational assets in these regions must potentially perform maneuvers to mitigate conjunctions. Rather than presenting high-precision analysis required for risk assessment and mitigation, this study builds upon the work of Anderson and Schaub [7], who illustrate a one-year, macroscopic congestion forecast for debris at GEO, to discern which *local* regions of the GEO ring are, in general, most susceptible to rising debris fluxes at different times. As overcrowding of GEO is becoming a serious concern for satellite owners internationally, knowledge of debris flux patterns—termed "debris weather"—is an imperative for space situational awareness at GEO. Figure 1 illustrates the complete RSO population at GEO (debris objects and controlled satellites) as of 01/01/13.

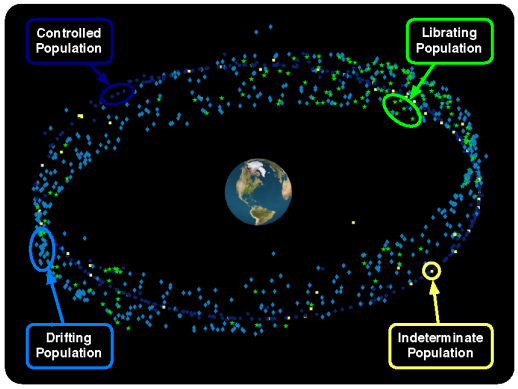


*Figure 1. Distribution of GEO population on 01/01/13.*

Existing debris analysis and evolution software [8, 9, 10] use inertial cell definitions to track debris cell passage events (CPE) arising from the intersections of osculating RSO orbits with the cells of interest during long-term propagation. Using various probability models, the associated spatial density and flux contributions for each CPE may thereafter be computed and implemented in collision risk assessment. For the GEO regime, these analysis tools often average over cell right ascension, providing debris fluxes as a function of altitude and declination [5]. Furthermore, employing inertially-fixed cell definitions only, flux contributions to particular GEO longitude slots at arbitrary times cannot be determined. Therefore, although *average* flux conditions at GEO may be estimated with such tools, *local* intersection events for certain longitude slots are not accessible – the latter is of significant interest to space operators concerned with the debris conditions in the vicinity of a functioning satellite. Furthermore, McKnight and Di Pentino [11] emphasize that fluxes averaged across longitude and time can grossly misrepresent short-term collision hazard, and as a consequence, alternative GEO collision hazard depictions that employ higher temporal and spatial resolutions should be adopted by the operator community. Following Anderson and Schaub [7], this study implements a toroidal cell configuration at the GEO altitude to evaluate the impact of the current RSO population—augmented under representative launch traffic models during long-term propagation—on each of the longitude slots at GEO, by performing a *near-miss anal-*

*Proc. '6th European Conference on Space Debris'*
*Darmstadt, Germany, 22–25 April 2013 (ESA SP-723, August 2013)*

*ysis* that attempts to assess the frequency at which uncontrolled objects pass within a given distance of a particular longitude slot. To enhance intuition, an integer number of near-misses is used here as the alternative to "typical" spatial density and flux metrics [5]. Population augmentation in the GEO ring has been investigated briefly in the literature [3, 5], albeit, these studies present debris fluxes averaged across longitude, altitude, and time, and thus do not address which longitude slots are the most prone to proliferating debris populations in the GEO environment.

Localized congestion forecasting for GEO is imperative, as it provides a metric as to how frequently satellite operators with assets in particular longitude slots will have to track nearby debris motion and potentially execute avoidance maneuvers. The latter is of particular importance, as avoidance maneuvers can temporarily force a satellite outside of its longitude slot, which may pose problems for the mission, and be difficult to manage if neighboring satellites are collocated in the same slot. Currently, the RSO population at GEO is sparse enough such that a simple time-shift of a scheduled maintenance maneuver is sufficient for evading debris; in these situations, no additional propellant is expended beyond that allocated for routine GEO station-keeping. However, as the GEO debris field continues to increase unchecked, the amount of propellant required to remain at a specified longitude slot while simultaneously mitigating conjunctions will begin increasing as well. The focus of this analysis is to illustrate "worst-case" debris congestion under a representative launch traffic model for a 50-year prediction period, and demonstrate that appropriate mitigation measures at end-of-life can serve to attenuate local debris congestion.

## 2. CURRENT RSO POPULATION AT GEO

The RSO population in the GEO regime is classified with a taxonomy used by the European Space Agency's DISCOS database (Database and Information System Characterising Objects in Space) [12]. For GEO RSOs, seven orbit categories are implemented for classifying the type of geosynchronous orbits traversed by these objects; Table 1 provides a description of this classification system. Geosynchronous RSOs are selected according to ESOC's *Classification of Geosynchronous Objects* reports [12]: (a) eccentricity smaller than $0.2$ ($e < 0.2$), (b) inclination smaller than $70^\circ$ ($i < 70^\circ$), and (c) mean motion between $0.9$ and $1.1$ revs per sidereal day ($0.9 < n < 1.1$).

Orbit data are obtained from publicly-available two-line element (TLE) sets provided by U.S. Strategic Command (USSTRATCOM).[1] For this debris flux study, a reference TLE set obtained on 01/01/13 is employed. TLE data are provided as doubly-averaged Keplerian elements [5] with mean motion instead of semi-major axis, transformed into Cartesian states in the true equator, mean equinox (TEME) frame [13] via SGP-4 theory [14] for this study.[2] Note that because of the limited accuracy of the TLE sets, these data are *not meant for high-precision analyses* – as the purpose of this study is to forecast near-miss events occurring on a macroscopic scale, the accuracy of these data is sufficient. Furthermore, as only objects larger than one meter are routinely tracked at the GEO altitude [12], only RSOs at least of this size are considered. Since this study only incorporates the trackable, catalogued, and unclassified GEO RSOs with up-to-date TLEs, the findings of this study serve to illustrate a conservative lower bound of the true debris congestion situation in the GEO ring.

## 3. FORECASTING LOCAL GEO CONGESTION

### 3.1. Formulation of Near-Miss Events

Near-miss events for the GEO longitude slots are determined by formulating a GEO-encompassing torus of major radius $r_{\text{GEO}} = 42164$ km and minor radius $\tilde{r}$ [7], partitioned into longitude increments of $\Delta\lambda = 1.0^\circ$. Minor radii of $\tilde{r} = 50/100/300/700$ km are simulated to evaluate the frequency of near-miss CPE occurring from distances representative of a $1^\circ$ longitude slot at GEO ($\sim$700 km) to distances at which precise conjunction assessment and analysis roughly could be considered ($\sim$50 km). Further, this torus formulation is a natural choice for evaluating CPE for the non-inertial GEO longitude slots, as this torus geometry is invariant as seen by both the inertial frame (J2000) and Earth-centered, Earth-fixed frames, in which these longitude slots are fixed [7].

Near-miss events are detected during propagation of an object by checking for the transversal of this GEO torus boundary at each time step during numerical integration. Mathematically, a near-miss event occurs if [7]

$$\left(r_{\text{GEO}} - \sqrt{r_X^2 + r_Y^2}\right)^2 + r_Z^2 - \tilde{r}^2 < 0 \qquad (1)$$

is satisfied, where $(r_X, r_Y, r_Z)^T$ is the RSO position vector expressed in the inertial frame. The longitude of intersection $\lambda_{\text{CPE}}$ is thus determined as [7]:

$$\lambda_{\text{CPE}} = \arctan\left(\frac{r_Y}{r_X}\right) - \alpha_G \qquad (2)$$

where $\alpha_G$ is the right ascension of Greenwich (i.e., Greenwich sidereal time) [16]. When a torus-intersection is detected with Equation (1), the longitude of intersection is determined with Equation (2), and the total near-miss count for the corresponding toroidal cell is updated. To ensure that equivalent intersection events are not accounted for more than once during CPE checking, counting logic is employed before a cell intersection counter is updated to "screen" the event for redundancy. The full algorithm for determining near-miss events with the torus formulation is detailed by Anderson and Schaub [7].

[1] Publicly-available TLE data sets (updated twice daily) are available for bulk download from: `https://www.space-track.org/`

[2] ANSI-C implementation of merged SGP-4/SDP-4 theory for TLE processing is available from: `http://www.sat.dundee.ac.uk/~psc/sgp4.html` [15]

*Table 1. Orbit classifications for geosynchronous objects in GEO congestion study.*

| Class | Type | Description |
|---|---|---|
| C1 | Controlled | Longitude/inclination control (E-W/N-S control) |
| C2 | Controlled | Longitude control only (E-W control only) |
| D | Drifting | Drift above/below/through protected GEO zone |
| L1 | Librating | Libration about Eastern stable point ($\lambda = 75°$E) |
| L2 | Librating | Libration about Western stable point ($\lambda = 105°$W) |
| L3 | Librating | Libration about Eastern/Western stable points |
| IN | Indeterminate | Unknown status (e.g., recent TLE not available) |

### 3.2. Propagator and Implementation

A special perturbations propagation routine implemented in ANSI-C and parallelized with the OpenCL architecture is implemented to propagate the uncontrolled GEO population and determine torus intersection events. Per implementation considerations of the OpenCL configuration,[3] a lower-fidelity—albeit representative—force model of the GEO environment is employed, with the added benefit of dramatically-decreased simulation run times. Here, the two-body equations of motion are numerically integrated under a $4 \times 4$ EGM-96 spherical harmonics expansion, luni-solar perturbations, and the "cannonball" solar radiation pressure (SRP) perturbation ("harshly" attenuated by the geometric occultation algorithm presented by Montenbruck and Gill [17]). The equations of motion are

$$\ddot{\boldsymbol{r}} = -\frac{\mu_\oplus}{r^3}\boldsymbol{r} + \boldsymbol{a}_\oplus + \boldsymbol{a}_{\leftmoon} + \boldsymbol{a}_\odot + \boldsymbol{a}_{\text{SRP}} \qquad (3)$$

where the first term denotes Keplerian two-body acceleration, $\boldsymbol{a}_\oplus$ is the acceleration due to the nonsphericity of Earth, $\boldsymbol{a}_{\leftmoon}$ and $\boldsymbol{a}_\odot$ are the third-body contributions from the Moon and Sun, respectively, and $\boldsymbol{a}_{\text{SRP}}$ is the SRP acceleration. Solar radiation pressure is modeled using the inverse-square diffusion formulation of solar luminosity $L_\odot \approx 3.839 \times 10^{26}$ J/s, using a coefficient of reflectivity $c_r \equiv 1.5$ and area-to-mass ratio $A_\odot/m = 0.04$ m$^2$/kg.[4]

In higher-fidelity force models, transformations between Earth-fixed and Earth-inertial frames incorporate accurate Earth orientation parameters (EOP) to account for the influence of precession, nutation, and polar motion, and software suites such as the SPICE toolkit may be employed to perform these complex coordinate transformations.[5] In this parallelized propagator, however, a lower-fidelity transformation that accounts strictly for a $z$-axis rotation by Greenwich sidereal time is implemented for purposes of increased speed at run time. Furthermore, instead of drawing the inertial Moon and Sun position vectors from the ephemerides, this routine implements low-precision formulae for the geocentric coordinates of these bodies, as stated in the 2013 *Astronomical Almanac* [19]. This propagator uses an eighth-order, predictor-corrector Gauss-Jackson integrator [20] initialized with the Prince-Dormand 8(7) algorithm for numerical integration of the equations of motion in Equation (3). During initial propagation of the debris field to the CPE start date, and during near-miss computations in the prediction span, a time step of ten minutes is specified for sufficient fidelity.[6] Validation of this lower-fidelity, parallel propagation routine has been performed against high-fidelity, sequential propagation, and the macroscopic congestion patterns predicted by these two propagation strategies differ insignificantly.

## 4. FORECASTING CONGESTION WITH POPULATION AUGMENTATION

### 4.1. Operational GEO Orbit Model

For more realistic, long-term congestion forecasting, the GEO RSO population must be meaningfully augmented to simulate nominal launch traffic for this regime. Realistic population augmentation necessitates an operational GEO orbit model to quantify *where* C1/C2 satellites are "typically" positioned at insertion into their designated longitude slots – such a model serves to generate the initial conditions for new controlled satellites created during long-term forecasting (the GEO launch instantiation procedure is outlined in Section 4.2). To construct this operational orbit model, data from the 01/01/13 reference TLE set, the *Space-Track Geosynchronous Report*[7], and the electronic *SatBeams* database[8] are compiled, yielding semi-major axis, eccentricity, inclination, and longitude information for 768 past and present GEO satellites (including all unclassified launches to GEO as of 01/01/13), and 94 GEO satellites planned through the year 2020. Employing these data, stacked histograms are generated for the semi-major axis, eccentricity, inclination, and geocentric longitude, and appropriate probability density functions are "fit" to these histograms (with trial-and-error) to construct representative distributions

[3] The *OpenCL 1.2 Specification* is available from Khronos Group at: `http://www.khronos.org/registry/cl/`.

[4] Schaub and Jasper [18] indicate that $A_\odot/m \approx 0.04$ m$^2$/kg is representative of the RSO population at GEO – this value is implemented within a "nominal" solar radiation pressure perturbation *for all* objects.

[5] The Jet Propulsion Laboratory's (JPL) SPICE toolkits are available from: `http://naif.jpl.nasa.gov/naif/toolkit.html`.

[6] Preliminary studies indicate that simulation results exhibit insignificant changes when smaller time steps (such as one minute) are utilized.

[7] The Space-Track Geosynchronous Report is available at: `https://www.space-track.org/perl/geo_report.pl`.

[8] The SatBeams database gives GEO satellite longitude and launch year information, and is available from: `http://www.satbeams.com/satellites`.

from which the orbital elements of a new controlled satellite may be drawn. Figure 2 shows these parameter histograms (stacked by launch decade) and their associated density functions, summarized for each element below:

- *Semi-major axis* $a$. Normal distribution with mean $\mu = 42164.8$ km and standard deviation $\sigma = 1$ km. The probability density function (PDF) and cumulative distribution function (CDF) for this distribution are given by (for $-\infty < x < \infty$):

$$f_{\mathcal{N}}(x;\mu,\sigma) = \frac{1}{\sigma\sqrt{2\pi}} \exp\left[-\frac{1}{2}\left(\frac{x-\mu}{\sigma}\right)^2\right] \quad (4)$$

$$F_{\mathcal{N}}(x;\mu,\sigma) = \frac{1}{2}\left[1 + \operatorname{erf}\left(\frac{x-\mu}{\sigma\sqrt{2}}\right)\right] \quad (5)$$

- *Eccentricity* $e$. Half-normal distribution derived from normal distribution with $\sigma = 5.0 \times 10^{-4}$, for which the PDF and CDF are given by (for $x \geqslant 0$):

$$f_{\mathcal{N}/2}(x;\sigma) = \frac{\sqrt{2}}{\sigma\sqrt{\pi}} \exp\left(-\frac{x^2}{2\sigma^2}\right) \quad (6)$$

$$F_{\mathcal{N}/2}(x;\sigma) = \operatorname{erf}\left(\frac{x}{\sigma\sqrt{2}}\right) \quad (7)$$

- *Inclination* $i$. Half-normal distribution derived from normal distribution with $\sigma = 0.08^\circ$.

- *Longitude* $\lambda$. Gaussian mixture of two wrapped normal distributions, using $(\mu_1, \sigma_1) = (55^\circ, 65^\circ)$ and $(\mu_2, \sigma_2) = (260^\circ, 25^\circ)$, mixed with the following:[9]

$$\lambda \Leftarrow 0.75 f_{\mathcal{W}}(\mu_1,\sigma_1) + 0.25 f_{\mathcal{W}}(\mu_2,\sigma_2) \quad (8)$$

where the PDF and associated CDF for the wrapped normal distribution are given by (for $0 \leqslant x \leqslant 2\pi$):

$$f_{\mathcal{W}}(x;\mu,\sigma) = \frac{1}{\sigma\sqrt{2\pi}} \times \sum_{k=-\infty}^{\infty} \exp\left[-\frac{(x-\mu+2\pi k)^2}{2\sigma^2}\right] \quad (9)$$

$$F_{\mathcal{W}}(x;\mu,\sigma) = \frac{1}{2}\sum_{k=-\infty}^{\infty}\left[\operatorname{erf}\left(\frac{x-\mu+2\pi k}{\sigma\sqrt{2}}\right) - \operatorname{erf}\left(\frac{-\mu+2\pi k}{\sigma\sqrt{2}}\right)\right] \quad (10)$$

For computer implementations, sampling from the distributions is performed by drawing a pseudo-random number on the interval $[0, 1]$ that represents the cumulative probability in the distribution, up to and including the desired value. Then, the appropriate CDF is back-solved for the value of $x$ that would yield this cumulative probability. Back-solving the wrapped normal CDF is performed by incrementally stepping through the interval $x \in [0, 2\pi]$ in Equation (10) until the value of the random number has been achieved to tolerance (it is sufficient to iterate $k$ as $k = -100 \ldots 100$).

The right ascension of the ascending node is selected uniformly on the interval $\Omega \in [0, 360^\circ]$, and the true anomaly $f = 0^\circ$, such that all new satellites are inserted at the perigee of their operational orbits. Then, the argument of perigee $\omega$ must satisfy

$$\omega = \alpha_G + \lambda - \Omega \quad (11)$$

where $\alpha_G$ is the right ascension of Greenwich, computed at the epoch of insertion. After the initial orbit elements have been sampled in this manner, the Keplerian elements are converted into a Cartesian state and assigned to the controlled satellite. This methodology ensures that new controlled satellites created during long-term forecasting exhibit initial orbit elements that are highly representative of operational GEO orbits harnessed since the first GEO utilization in 1963.

### 4.2. Business as Usual without Mitigation

Launches to operational GEO orbits are simulated with the probabilistic, "open-loop" event instantiation method as implemented in the European Space Agency's DELTA (Debris Environment Long-Term Analysis) tool [5]. Following Klinkrad [5], the probability $\mathcal{P}_j$ of $j$ launches occurring in a given analysis interval is modeled with the Poisson distribution

$$\mathcal{P}_j = \frac{c^j}{j!}\exp(-c) \quad (12)$$

where the parameter $c$ is the average number of launches occurring during the analysis interval, computed as $c =$ (average annual launch rate to orbit regime [years$^{-1}$]) $\times$ (length of analysis interval [years]) [5]. Assuming the "business-as-usual" GEO launch rate of 30 satellites per year [3, 5] and with one-day analysis intervals, $c \approx 0.082$ as a first approximation for typical GEO launch traffic. For computer implementations, the probabilities $\mathcal{P}_j$ for $j = 0, 1, \ldots, k$ are first determined until a "threshold" value $\epsilon$ is achieved, such that $\mathcal{P}_{k+1} \leqslant \epsilon$ (for this study, $\epsilon = 10^{-6}$ is used). The resultant probabilities $\mathcal{P}_j$ are then normalized such that their sum is equal to 1:

$$\hat{\mathcal{P}}_j = \frac{\mathcal{P}_j}{\sum_{i=0}^{k}\mathcal{P}_i} \implies \sum_{j=0}^{k}\hat{\mathcal{P}}_j = 1 \quad (13)$$

A pseudo-random number $\hat{\zeta}$ on the interval $[0, 1]$ is now drawn, and the number of launch occurrences in the analysis interval is thus determined by the largest $j$ for which the sum of the normalized probabilities $\hat{\mathcal{P}}_j$ is still less than $\hat{\zeta}$, i.e.,

$$\sum_{i=0}^{j}\hat{\mathcal{P}}_i \leqslant \hat{\zeta} < \sum_{i=0}^{j+1}\hat{\mathcal{P}}_i \quad (14)$$

[9] A Gaussian mixture is implemented to simulate the "bimodality" of the longitude histogram in Figure 2(d), i.e., high concentrations of operational satellites above Europe/Asia and North America, but minimal assets above the Atlantic and Pacific Oceans.

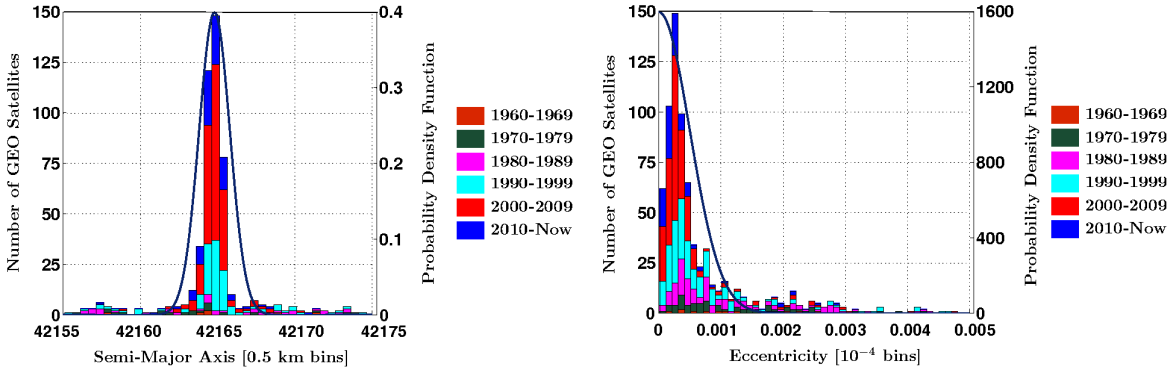


(a) Semi-major axis PDF for operational GEO orbit.




(b) Eccentricity PDF for operational GEO orbit.

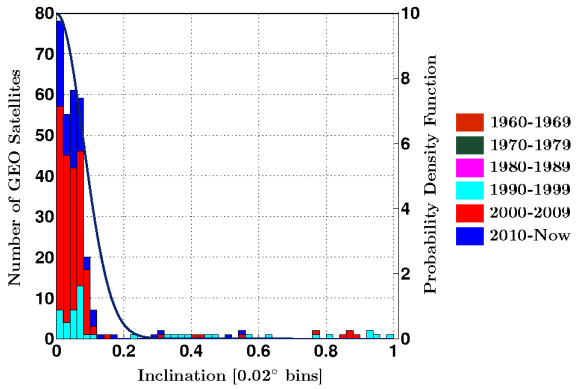


(c) Inclination PDF for operational GEO orbit.

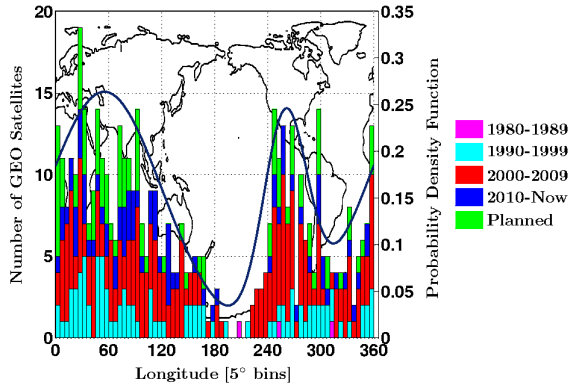


(d) Longitude PDF for operational GEO orbit.

*Figure 2. Parameter distributions for representative sampling of operational GEO orbits.*

Therefore, following each day of propagation, a pseudo-random number $\hat{\zeta}$ is drawn, and the number of launches during the past day is determined with Equation (14). If a successful launch has been initiated, a controlled GEO satellite (C1) is created, and the initial orbit elements are sampled from the representative distributions presented in Section 4.1. For the purposes of this study, the new C1 satellite is "injected" into its orbit at midnight, and it is assigned a nominal lifetime of 15 years.[10] Controlled satellites that reach end-of-life (EOL) during propagation are deactivated without any attempt at re-orbiting – these satellites are labeled as indeterminate (IN) and added to the uncontrolled RSO population for propagation.

Although the "business-as-usual" launch rate of 30 new GEO satellites per year offers a suitable first approximation for long-term congestion forecasting in this arena, it is more instructive to consider the more realistic case of an increasing launch rate to operational orbits at GEO. Figure 3 illustrates the number of launches to GEO occurring every year since 1963, using data compiled from the *Space-Track Geosynchronous Report*. Observing that the number of launches $N_L$ is approximately proportional to the launch year $t_L$, simple linear regression provides the following linearly-increasing GEO launch traffic model:

$$N_L = 0.62 t_L - 1218 \text{ [launches/year]} \qquad (15)$$

To implement this launch traffic model, the parameter $c$ is updated after every year of propagation, and the probabilities in Equations (12)-(14) are recomputed to reflect a linearly-increasing launch rate. Figure 4 illustrates local congestion for the 01/13 - 01/63 prediction span, assuming this "business-as-usual" model in the absence of mitigation measures. Figure 4(a) illustrates the absolute number of near-miss events per day for the 50 km GEO torus, while Figure 4(b) quantifies increase in the mean number of near-miss events per day (averaged over each year of propagation) over the idealized "no future launches" traffic scenario (similar results are provided in Figure 4 for the 100/300/700 km radius cases). As anticipated, the strength of the debris weather increases with the torus radius $\tilde{r}$, and local congestion in the vicinity of the Eastern and Western gravitational wells dramatically expands as propagation time progresses.[11] "Bunching" of uncon-

[10]The baseline C1/C2 population in the 01/01/13 TLE set is also assigned this nominal lifetime (the COSPAR designation provides launch year). Wegener et. al. [3], and McKnight and Di Pentino [11], state that the average design lifetime of GEO satellites has continued to increase since 1964; extended lifetimes are not simulated here.

[11]McKnight and Di Pentino [11] estimate that the probability of collision at GEO is currently *seven times greater* near the E/W stable points.

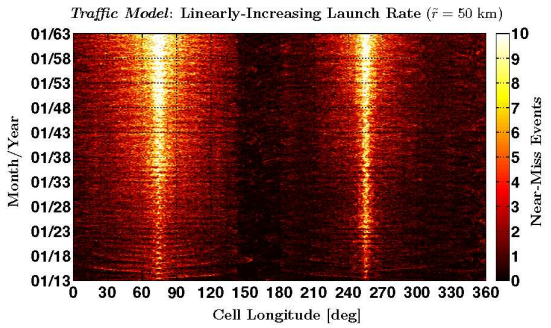


(a) Near-miss CPE forecasting for 01/13 - 01/63 for 50 km torus.

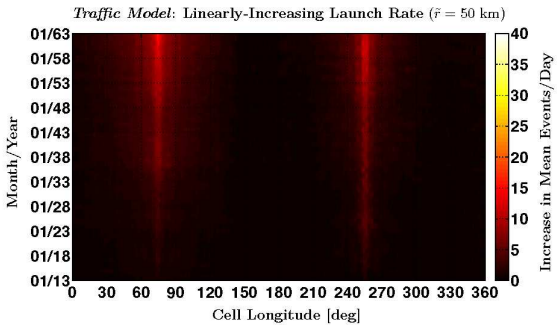


(b) Increase in near-miss events over "no future launches" scenario.

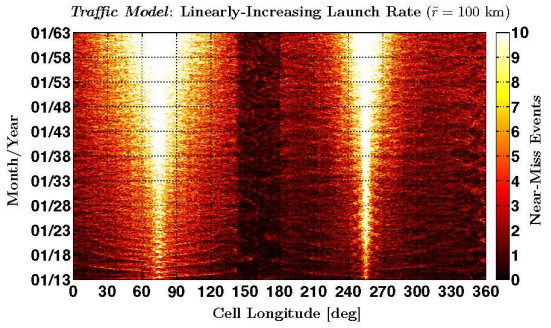


(c) Near-miss CPE forecasting for 01/13 - 01/63 for 100 km torus.

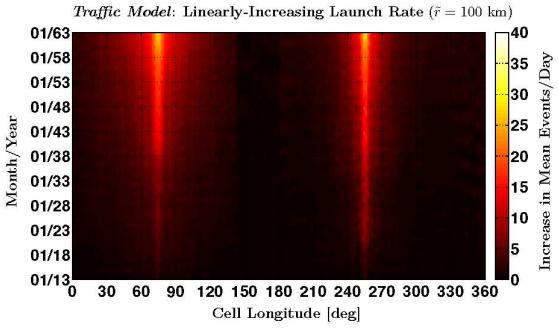


(d) Increase in near-miss events over "no future launches" scenario.

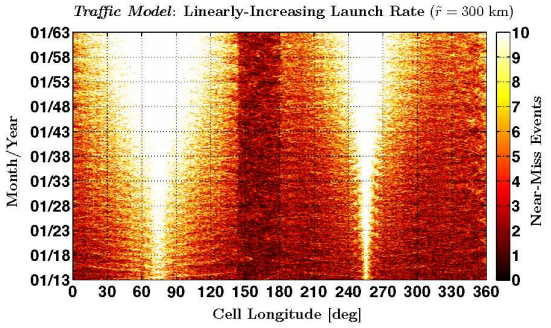


(e) Near-miss CPE forecasting for 01/13 - 01/63 for 300 km torus.

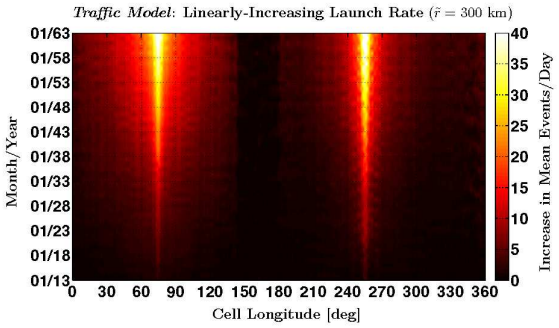


(f) Increase in near-miss events over "no future launches" scenario.

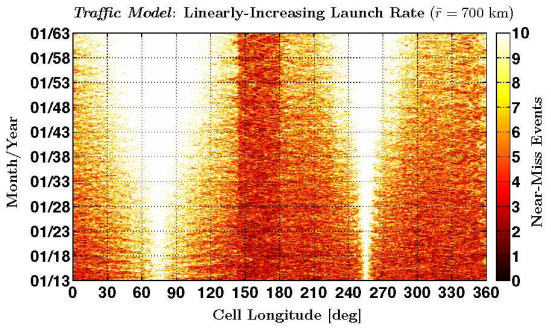


(g) Near-miss CPE forecasting for 01/13 - 01/63 for 700 km torus.

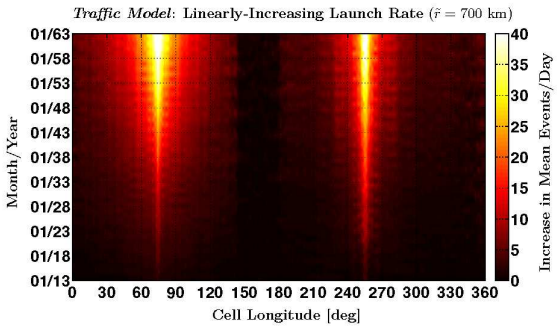


(h) Increase in near-miss events over "no future launches" scenario.

*Figure 4. 50-year congestion forecasting in the GEO ring, assuming linearly-increasing launch traffic model.*

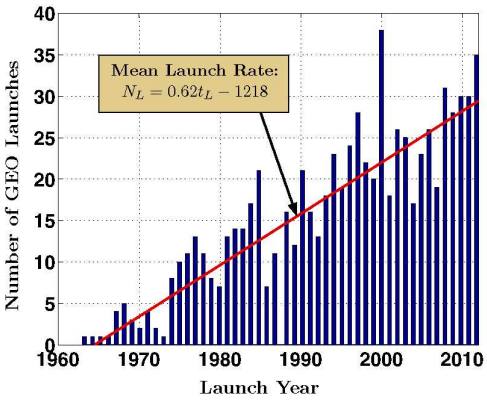


*Figure 3. History of launches to GEO orbit.*

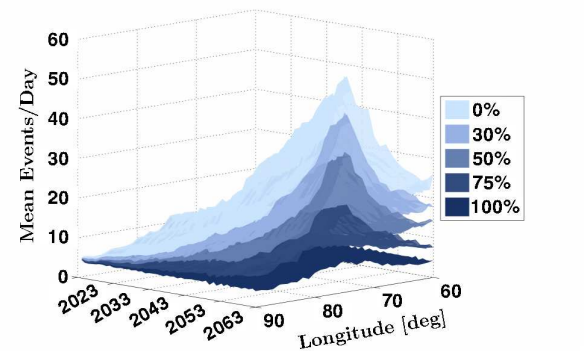


*Figure 5. Effect of "perfect" mitigation on congestion around Eastern gravitational well (300 km GEO torus).*

trolled objects around these gravitational wells is a well-known result, as is discussed by Luu and Sabol [21] and Chobotov [22] – this is a particularly troublesome result, as operating GEO satellites are typically inserted into longitude slots in these regions (see Figure 2(d)). Assets residing in the longitude interval $\lambda \in (60^\circ, 90^\circ)$ around the Eastern gravitational well will be subjected to upwards of 30 additional 700 km near-miss events per day on average by the year 2063. This is a striking finding that begins to corroborate the hypothesis that as the uncontrolled RSO population near GEO continues to increase, the amount of propellant required for routine station-keeping will rise in tandem, to account for increasing frequencies of debris avoidance maneuvers. Again, as uncontrolled debris objects smaller than one meter—although prevalent at GEO and only recently characterized with sufficient fidelity to incorporate in conjunction assessment [11]—are not considered in this study, this is an optimistic prediction of the true congestion situation in the GEO ring.

### 4.3. Business as Usual with Perfect Mitigation

The congestion forecasting performed thus far within this study has not yet addressed the influence of properly-implemented mitigation measures for C1/C2 satellites reaching EOL. Classic mitigation for the GEO regime incorporates re-orbiting to "graveyard" disposal orbits at perigee altitudes above the GEO ring, factoring the "protected" GEO zone and area-to-mass-ratio of the satellite into the minimum altitude calculation [1, 6, 23], per the re-orbiting guidelines of the Inter-Agency Space Debris Coordination Committee (IADC) [24]. To emphasize the importance of EOL mitigation measures for GEO satellites, this study assumes "perfect" mitigation, in which $N\%$ of C1/C2 assets achieving EOL are successfully re-orbited to circular orbits at altitudes that *do not interfere* with the GEO altitude in the prediction spans considered.

Figure 5 illustrates the influence of perfect mitigation on congestion in the neighborhood of the Eastern stable point, for $0\%$ (equivalent to the "business-as-usual" scenario in Figure 4), $30\%$, $50\%$, $75\%$, and $100\%$ mitigation (equivalent to the "no future launches" scenario), for a GEO torus radius of 300 km. As this perfect mitigation rate increases, the "congestion peak" centered around this gravitational well diminishes to the level of the idealized "no future launches" traffic scenario. It is instructive to recall that the case of $30\%$ mitigation was the most representative of the mitigation rate implemented for the GEO regime during the 1997-2003 time frame [1, 5]; of the 103 satellites that achieved EOL in this period, 34 were successfully re-orbited to IADC-compliant disposal orbits, 35 attempted re-orbiting, but resulted in orbits with insufficient perigee altitudes, and 34 were abandoned in libration orbits about the Eastern/Western stable points [1]. Low compliance may be attributed to (a) the sizable propellant cost for meeting the IADC re-orbit guidelines,[12] (b) the difficulty of estimating on-board propellant, and translating a computed re-orbit $\Delta v$ into a required fuel mass [5], or (c) older, retiring satellites that were designed and built before establishment of the IADC guidelines, for which successful execution of the required re-orbit maneuver was not often achievable [25].

Recently, however, Johnson [25] praises the strong support of the satellite operator community for preservation of the GEO regime. Of the 160 operational GEO satellites that achieved EOL in the period 2001-2010, approximately $80\%$ re-orbited to disposal orbits – of these satellites, $70\%$ were transferred to orbits at least 200 km above the GEO ring, and almost $50\%$ achieved at least 300 km above GEO, for compliance with the IADC re-orbiting guidelines [25]. As Figure 5 illustrates the imperativeness of properly-executed mitigation maneuvers, and how re-orbiting serves to attenuate congestion in a "business-as-usual" traffic scenario, these recent re-orbiting statistics are promising in that they suggest increased adherence to mitigation guidelines—and ultimately—a growing international desire to safeguard the delicate GEO ring.

[12] Klinkrad [5] indicates that a typical EOL re-orbit requires a $\Delta v$ of roughly 11 m/s, about 2.3% of the entire station-keeping budget for a 10-year mission.

## 5. CONCLUSION

Forecasting of localized debris congestion in the geosynchronous environment is performed to quantify the number of near-miss events occurring for each longitude slot in this regime. A parallelized, reduced-fidelity propagation routine is implemented in tandem with a geostationary torus configuration and publicly-available TLE data to simulate congestion in "no future launches" and "business-as-usual" launch traffic scenarios, with and without perfect mitigation at end-of-life. Results indicate that debris congestion in the vicinity of the two gravitational wells will become severe inasmuch as mitigation guidelines for this regime are not globally adhered to. Fortunately, a burgeoning desire to preserve GEO is reflected in the increasing numbers of satellite operators attempting re-orbit at EOL. Ultimately, these mitigation measures must be combined with active removal and remediation at GEO, to protect the future usefulness of this natural resource and driver for space development, and preclude a situation similar to that now sustained in LEO.

## ACKNOWLEDGEMENTS

The authors would like to acknowledge Brandon Jones and his TurboProp software [26], from which the integration routines employed in this research were obtained.

## REFERENCES

1. R. Jehn, V. Agapov, and C. Hernandez. The situation in the geostationary ring. *Advances in Space Research*, 35:1318–1327, 2005.
2. N.L. Johnson. Protecting the geo environment: Policies and practices. *Space Policy*, 15:127–135, 1999.
3. P. Wegener, J. Bendisch, H. Krag, M. Oswald, and S. Stabroth. Population evolution in the geo vicinity. *Advances in Space Research*, 34:1171–1176, 2004.
4. T. Yasaka, T. Hanada, and H. Hirayama. Geo debris environment: A model to forecast the next 100 years. *Advances in Space Research*, 23(1):191–199, 1999.
5. H. Klinkrad. *Space Debris: Models and Risk Analysis*. Praxis Publishing, 2006.
6. Rudiger Jehn and Cristina Hernandez. International practices to protect the geostationary ring. *Space Debris*, 1:221–233, 2001.
7. Paul V. Anderson and Hanspeter Schaub. Local orbital debris flux study in the geostationary ring. *Advances in Space Research*, 2013. doi: `http://dx.doi.org/10.1016/j.asr.2013.01.019`.
8. J.-C. Liou, D. T. Hall, P. H. Krisko, and J. N. Opiela. Legend: A three-dimensional leo-to-geo debris evolutionary model. *Advances in Space Research*, 34:981–986, 2004.
9. J. Bendisch, K. Bunte, H. Klinkrad, H. Krag, C. Martin, H. Sdunnus, R. Walker, P. Wegener, and C. Wiedemann. The master-2001 model. *Advances in Space Research*, 34:959–968, 2004.
10. H.G. Lewis, G. Swinerd, N. Williams, and G. Gittins. Damage: A dedicated geo debris model framework. In *Proceedings of the Third European Conference on Space Debris*, volume 1. ESA Publications Division, March 2001.
11. Darren S. McKnight and Frank R. Di Pentino. New insights on the orbital debris collision hazard at geo. *Acta Astronautica*, 85:73–82, 2013.
12. T. Flohrer. Classification of geosynchronous objects: Issue 14. Technical Report 1, European Space Operations Centre, February 2012.
13. David Vallado. *Fundamentals of Astrodynamics and Applications*. Microcosm Press, 3 edition, 2007.
14. Felix R. Hoots and Ronald L. Roehrich. Spacetrack report no. 3: Models for propagation of norad element sets. Technical report, Office of Astrodynamics, Aerospace Defense Center, December 1980.
15. David A. Vallado, Paul Crawford, Richard Hujsak, and T. S. Kelso. Revisiting spacetrack report no. 3: Revision 2. In *Proceedings of the 2006 AIAA/AAS Astrodynamics Specialist Conference*, August 2006.
16. Howard Curtis. *Orbital Mechanics for Engineering Students*. Elsevier Butterworth-Heinemann, 2005.
17. Oliver Montenbruck and Eberhard Gill. *Satellite Orbits: Models, Methods, Applications*. Springer, 2000.
18. Hanspeter Schaub and Lee E. Z. Jasper. Circular orbit radius control using electrostatic actuation for 2-craft configurations. In *Proceedings of the 2011 AAS/AIAA Astrodynamics Specialist Conference*, August 2011.
19. *The Astronomical Almanac for the Year 2013*. United Kingdom Hydrographic Office, 2013.
20. Matthew M. Berry and Liam M. Healy. Implementation of gauss-jackson integration for orbit propagation. *Journal of the Astronautical Sciences*, 52(3):331–357, July-September 2004.
21. Kim Luu and Chris Sabol. Effects of perturbations on space debris in supersynchronous storage orbits. Technical report, Air Force Research Laboratory, October 1998.
22. Vladimir A. Chobotov, editor. *Orbital Mechanics*. American Institute of Aeronautics and Astronautics, Inc., 3 edition, 2002.
23. NASA. Process for limiting orbital debris. NASA-STD-8719.14 Change 4, National Aeronautics and Space Administration, September 2009.
24. IADC/WG4. Iadc space debris mitigation guidelines. Technical report, IADC, September 2007.
25. Nicholas L. Johnson. A new look at the geo and near-geo regimes: Operations, disposals, and debris. *Acta Astronautica*, 80:82–88, June 2012.
26. Keric Hill and Brandon A. Jones. *TurboProp Version 4.0*. Colorado Center for Astrodynamics Research, University of Colorado at Boulder, May 2009.